

Continuous Wave Operation and Mode-Locking of Ti:Sapph Lasers

Michael Meehan

A senior thesis submitted to the faculty of  
Brigham Young University  
in partial fulfillment of the requirements for the degree of

Bachelor of Science

John Colton, Advisor

Department of Physics and Astronomy

Brigham Young University

June 2016

Copyright © 2016 Michael Meehan

All Rights Reserved

## ABSTRACT

### Continuous Wave Operation and Mode-Locking of Ti:Sapph Lasers

Michael Meehan

Department of Physics and Astronomy, BYU

Bachelor of Science

Titanium-sapphire lasers are useful in condensed matter research because of their ability to be mode-locked, generating ultrafast, regular pulses of coherent radiation. When designing Ti:sapph lasers, their stability in continuous wave (CW) operation is often overlooked; however, this feature is often useful and would make a Ti:sapph laser more versatile. We discuss implementing an alternative laser cavity design that provides more stability in CW operation while retaining the ability to be mode-locked.

Keywords: Ti:sapph, laser, mode-locked, continuous wave

# Contents

<b>Table of Contents</b>	<b>iii</b>
<b>List of Figures</b>	<b>iv</b>
<b>1 Background</b>	<b>1</b>
1.1 Ti:sapphire Lasers . . . . .	1
1.2 Applications . . . . .	2
1.3 Overview . . . . .	3
<b>2 Methods</b>	<b>4</b>
2.1 Laser Design . . . . .	4
2.2 Laser Operation . . . . .	7
<b>3 Results</b>	<b>10</b>
<b>Appendix A ABCD Matrix Calculation</b>	<b>14</b>
<b>Bibliography</b>	<b>18</b>

# List of Figures

2.1	Prism-based laser design . . . . .	5
2.2	Alternative laser design . . . . .	5
2.3	Curved mirror in CW operation . . . . .	6
3.1	Stability Scan . . . . .	11
3.2	Power Distribution . . . . .	12
A.1	<b>ABCD matrix for distance <math>d</math></b> . . . . .	15
A.2	<b>ABCD matrix for mirror with focal length <math>f</math></b> . . . . .	15
A.3	<b>Stability ABCD matrix:</b> This represents a full beam round-trip. By using values in tables A.1 and A.2 and inserting into the matrices in figures A.1 and A.2, the final matrix is obtained with matrix multiplication. . . . .	16
A.4	<b>Beam size ABCD matrix:</b> This represents the beam path from new HR to OC. By using values in tables A.1 and A.2 and inserting into the matrices in figures A.1 and A.2, the final matrix is obtained with matrix multiplication. . . . .	16
A.5	<b>Beam size calculation:</b> By multiplying the paraxial ray vector by the beam size matrix in figure A.4 on the left, we can predict the ray behavior at the output coupler. . . . .	17

# Chapter 1

## Background

### 1.1 Ti:sapphire Lasers

While the theoretical groundwork for lasers was laid by Einstein in 1917, the first operational laser didn't come until 1960 with the work of Theodore Maiman. Maiman utilized a sapphire ( $\text{Al}_2\text{O}_3$ ) crystal doped with chromium. Soon after, P.F. Moulton demonstrated a laser which used titanium-doped sapphire ( $\text{Ti}:\text{Al}_2\text{O}_3$ ) instead of chromium and was tunable across a wide spectrum of wavelengths. Titanium sapphire lasers, or Ti:sapphs, operate between 660 and 1180 nm, the largest tuning range of any laser [1]. Because of this, Ti:sapphs are extremely useful in research, allowing researchers to finely control the output wavelength.

The broad spectrum of wavelengths affords another advantage: the ability to create ultrashort pulses of light via a process known as mode-locking. Within a laser, light reflects back and forth along the optical cavity. Since light is a wave, it interferes with itself creating standing waves called modes (much like vibrational modes in a string). The frequencies of these modes form a discrete set and are a function of the length of the optical cavity. In normal laser operation, known as continuous wave (CW) operation, each of these modes oscillates independently of each

other. However, when each mode is "locked" with a specific phase relationship to every other mode, the output of the laser will periodically interfere constructively and destructively, generating a periodic, pulsed output. The separation between pulses corresponds to the time it takes light to travel one round trip of the optical cavity, given by  $\tau = 2L/c$ . The duration of the pulses is inversely proportional to the mode-locked bandwidth,  $N/\tau$ , where  $N$  is the number of locked modes [2].

Designing and operating a mode-locked laser involves a large number of deeply connected design parameters along with nonlinear effects that create a chaotic engineering task [3]. The problem is further complicated if CW operation is desired in addition to mode-locking. Moulton's original Ti:sapph itself was subject to scattering and other issues making it only functional in pulsed operation and it would be years before high enough quality of crystal was produced for room-temperature CW operation [1]. Researchers in the High-Intensity Physics Laboratory at Washington State University prepared a set of guidelines for constructing a mode-locked Ti:sapph laser [4] on which our home-built Ti:sapph laser is based. However, these guidelines are sparse in instructions for laser operation and the laser design itself is subject to the same CW operation stability issues found in the earliest Ti:sapphs.

## 1.2 Applications

Previously our laboratory has used Ti:sapphs in a number of condensed matter experiments. One research used a Ti:sapph as a reference pulse in time-correlated single photon counting to measure the photoluminescence of quantum dots. By splitting the output beam of the laser, a portion of the beam was used to excite a sample while the other portion provided a precise temporal reference. In this experiment, the laser was mode-locked and generated pulses that were around five orders of magnitude faster than the photoluminescence lifetimes, approximating instantaneous excitation in the samples [5].

Our lab has also used Ti:sapphs in electron spin-lifetime experiments. For example, gallium arsenide (GaAs) has a band gap of 818.5 nm, within the operating wavelengths of Ti:sapph lasers. By pumping GaAs quantum wells, spin information was encoded on a sample and, using a second probe laser, the rate of decay of this spin was measured optically [6].

## 1.3 Overview

In addition to commercially-built lasers, our laboratory uses a Ti:sapph laser built in-lab based on the guidelines published by the Washington State University researchers. Use of this laser is hindered by lack of documentation. Furthermore, most of the existing knowledge of operation is passed on researcher to researcher as a working laser configuration evolved within our lab. No repeatable alignment procedure or diagnostics exists for this laser. Initially this thesis hoped to codify instructions for operation; however, the process proved to be too chaotic to describe with a high degree of rigor. Instead, this thesis aims to lay a groundwork for future researchers working with this laser and mitigate some of the trial-and-error associated with its operation, as best as possible.

Furthermore, this thesis aims to address part of the instability issue with CW operation. In doing so, we propose an alternative design to the original cavity and compare the stability as well as discuss mode-locking with both designs.

# Chapter 2

## Methods

### 2.1 Laser Design

The original configuration of the laser consists of 2 end-mirrors, one an output coupler and the other a high reflector, two high reflectors which focus into the Ti:sapph crystal, and two prisms between the crystal's mirrors and the other high reflector, as shown in figure 2.1. While potential dimensions are provided in the guidelines document, they are not meant to represent precise values and serve primarily as starting points [4]. The laser itself is pumped by a green diode-pumped solid state laser (DPSS) that enters through HR A on the side of the output coupler. Additionally, part of the beam path is diverted through a grating and into a charge-coupled device (CCD) which allows for rough measurements of the wavelength and bandwidth of the laser.

Alternatively, by bypassing the prisms and inserting a new, curved high reflector as depicted in figure 2.2 the overall path length can be decreased while potentially increasing operational stability. By using ABCD matrix formalism [7], we calculated the optimal specifications for the new high reflector (see Appendix A). Figure 2.3 plots the distance to the high reflector versus the focal length necessary for optimal stability. By choosing a focal length of 200 mm, we know where to place

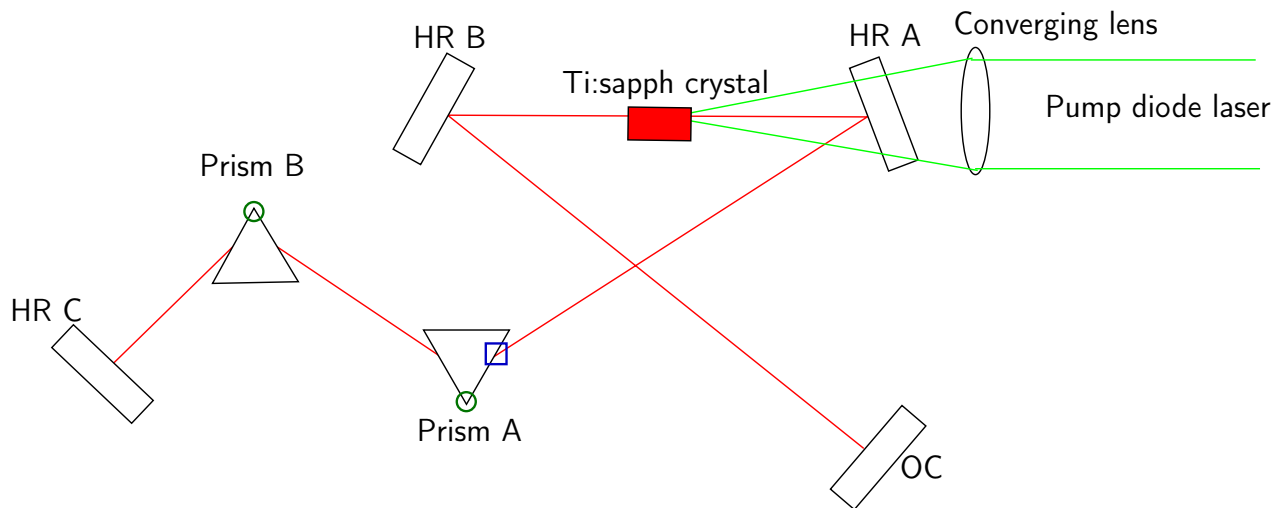


**Figure 2.1 Prism-based laser design:** A green DPSS stimulates emission from the Ti:sapph crystal. When the optical path is aligned correctly, the IR light lases out the output coupler. Not to scale.

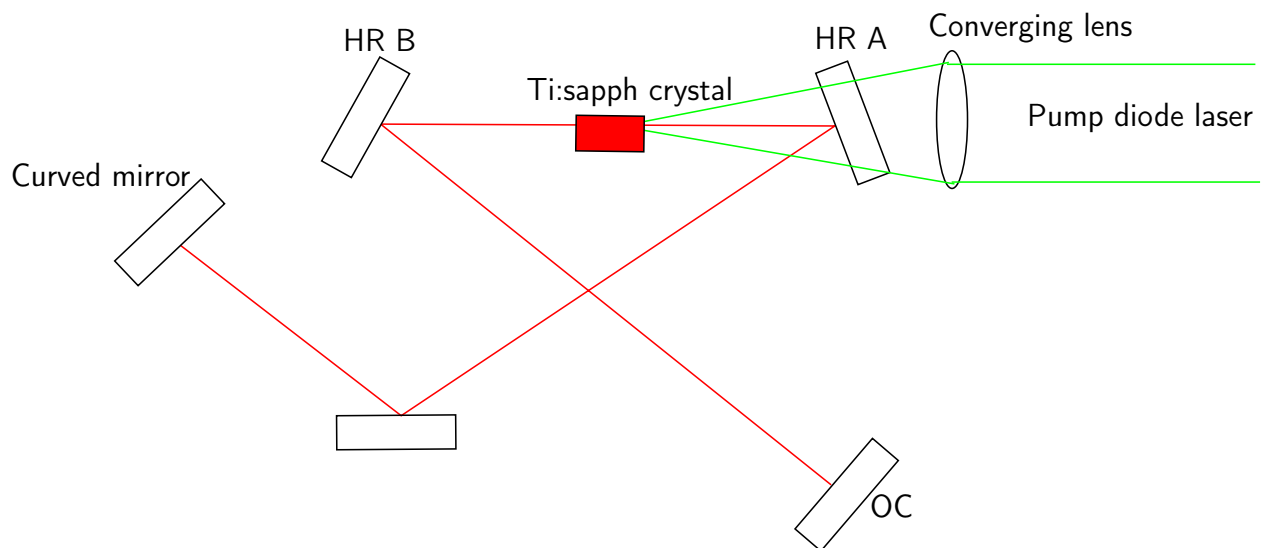


**Figure 2.2 Alternative laser design:** The overall setup gives a reduced optical path. The unlabeled mirror is a flat mirror that redirects the beam so it remains on the optical table. Not to scale.

the new high reflector in our laser cavity.

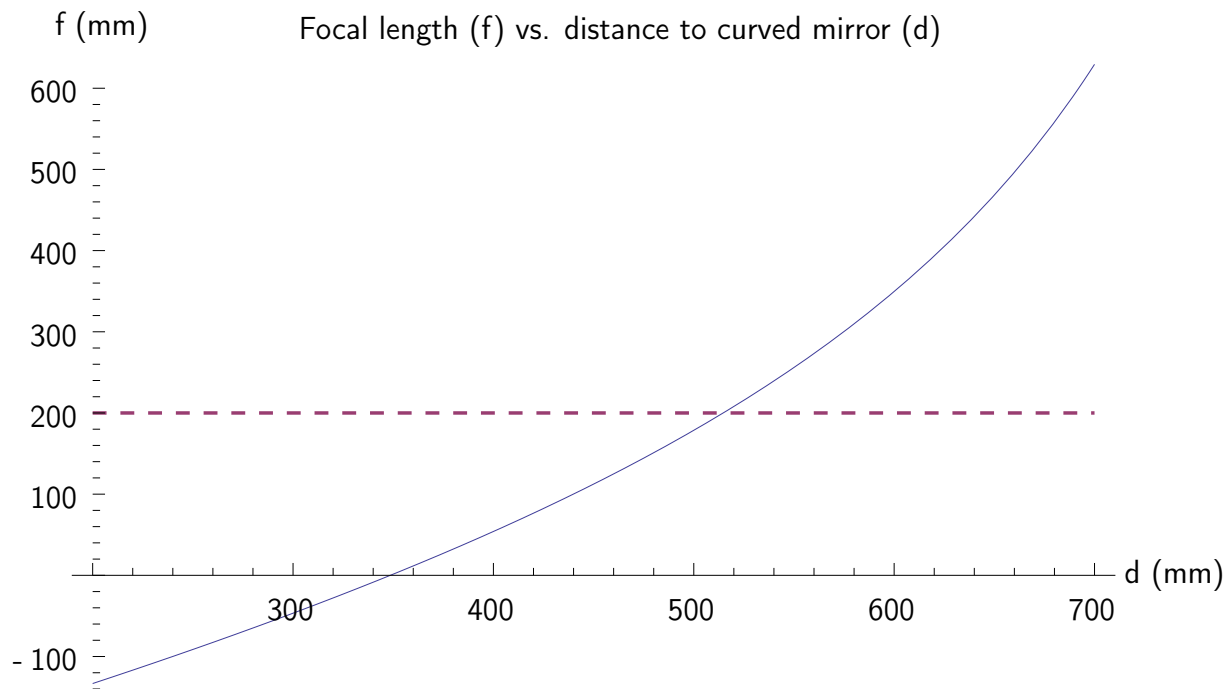


**Figure 2.3 Curved mirror in CW operation:** The distance to the curved mirror depends on the optimal focal length of the mirror. The distance used in the alternative setup corresponds to a focal length of 200 mm, the focal length of the mirror available to us, represented by the dashed line.

## 2.2 Laser Operation

In order to achieve lasing, the optical path must be aligned so that incident light on the output coupler is reflected back along its incident path. However, the light being aligned is not visible and while the visible green pump laser dominates what is seen by the naked eye, it does not follow the same path as the IR laser light. In the initial step of alignment the IR light is powerful enough to be detected with orange goggles; however, later alignments require the aide of an IR scope. A prescriptive summary for aligning and mode-locking the laser, using mirror notation from figure 2.1, follows.

### Laser alignment

**HR B/OC alignment** View the reflection from HR B on OC through goggles that filter out green light. Adjust HR B enter the brightest visible object on the OC.

**Prism alignment** If the laser has been mode-locked, the prisms will not be in an optimal position for initial lasing alignment. Using an IR scope, trace the beam path from HR A to prism A. Position prism A so that the beam strikes approximately twice as close to the inward-facing face than the outward-facing vertex (see the square on prism A in figure 2.1).

**HR A/HR C alignment** View the beam from the prisms on HR C with an IR scope. After passing through the prisms the beam appears rectangular. Adjust HR A to center the rectangle on HR C as well as the intensity of the light in the rectangle.

**Ends alignment** While viewing OC with an IR scope, adjust HR C so that the reflection reaches OC. Perturbing HR C should affect a change in what is viewed on OC. If not, the previous steps may need to be repeated. Align the reflection from HR C with the initial reflection from HR B. Repeat this while viewing HR C and adjusting OC. This step may take several iterations switching back and forth.

**Lasing** When the ends are aligned sufficiently so that the light is close to following the same path from HR C to OC and from OC to HR C, observing the output past OC should reveal two beams, one of which moves as HR C is moved. Adjust HR C to align these two beams. When the beams are close to overlapping it should lase. When lasing is achieved there will be a marked increase in intensity.

**Optimization** The output power of the laser can be optimized by adjusting the alignment of HR C and OC. Use an optical power meter to measure the intensity of the output of the laser and adjust HR C and OC to maximize the measured intensity. Decrease the pump laser's power until lasing is only barely achieved and repeat until the pump laser's power can no longer be lowered.

**Cleaning optics** If lasing doesn't occur at a moderate pump power or if a large amount of specular reflection is observed from any of the optics, it is helpful to thoroughly clean the optics and restart the alignment process.

### **Mode-locking**

Mode-locking is achieved once the laser is lasing by tweaking the prisms and crystal's mirrors while observing the bandwidth read by the CCD. The main adjustments are to the prisms and typically require the prisms to be moved so that the beam path is closer to the outward-facing vertices (denoted by circles in figure 2.1). As slight adjustments are made to the prism and mirror positions as well as the alignment of the high reflector end-mirror, slightly perturb the output coupler with a wooden mallet. Unfortunately there is not a rigorous method by which to achieve mode-locking. However, when it does occur, the CCD will change from a bright line to a bright smearing of frequencies.

In order to measure and compare the stability of the configurations, we placed a photodiode behind an neutral density filter to measure the output of the laser. The laser was adjusted to maximize the output intensity at the lowest possible input power that still achieved lasing. Then the input power was set to 3.5 W and the output intensity was measured and recorded by a LabVIEW interface sampling 5000 times at a rate of one sample per second.

# Chapter 3

## Results

Over a period of approximately 85 minutes we measured the filtered power of the Ti:sapph laser (see figure 3.1) at an average of  $0.3148 \mu\text{W}$  with a standard deviation  $0.0355 \mu\text{W}$ . The data points do not seem to be uniformly distributed and a histogram of the intensities (see figure 3.2) shows two peaks, a wide peak at lower intensities and a narrower peak at higher intensities. The power of the laser seemed to drift to a higher level at some point during the measurement. The average power of the first 2500 points was  $0.2872 \mu\text{W}$  with a standard deviation of  $0.0245 \mu\text{W}$  while the latter 2500 points had an average power of  $0.3424 \mu\text{W}$  with a standard deviation  $0.0201 \mu\text{W}$ . These two averages are close to the observed peaks in the histogram plot.

While the ABCD matrix calculation supported the theory of a stable CW operation of the laser we neglected to consider the size of the reflected beam on the output coupler in the alternative configuration of the laser. When attempting to get the laser to lase in that setup the mirrors seemed to be angled correctly; however, the beam was not visible on the output coupler. Revisiting the calculations we calculated that the beam should have a radius of 0.163 meters at the output coupler, as shown in Appendix A. By adjusting the planned distance between the new HR (labeled as curved mirror in figure 2.2) and the flat mirror we attempted to determine a configuration that would result in both stable lasing as well as a small beam width within the physical constraints of the optics table

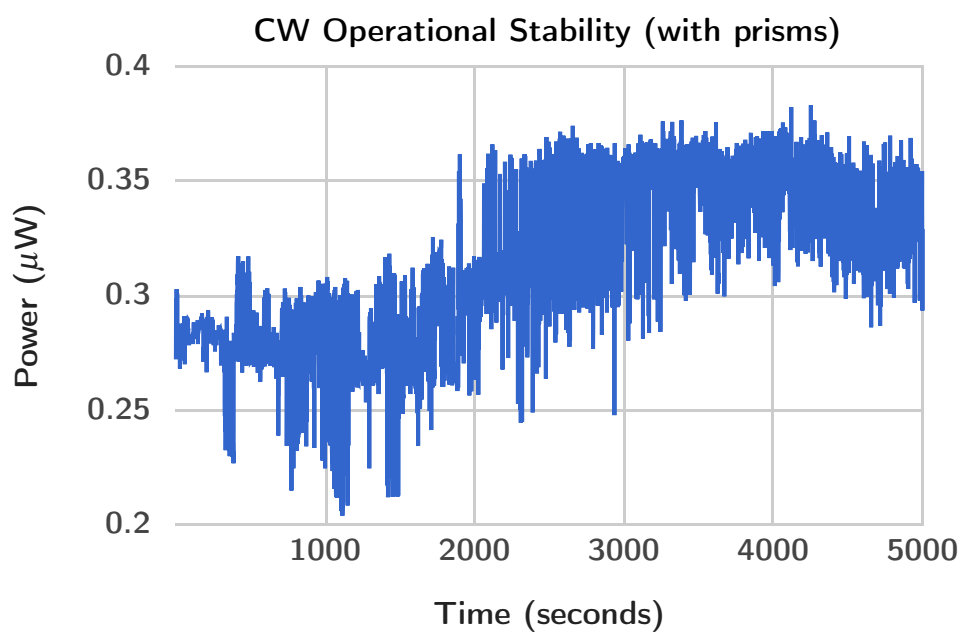


**Figure 3.1 Laser stability scan:** The power of the laser was measured 5000 times at a rate of one measurement per second. There appears to be a shift in average power after 2000 seconds.

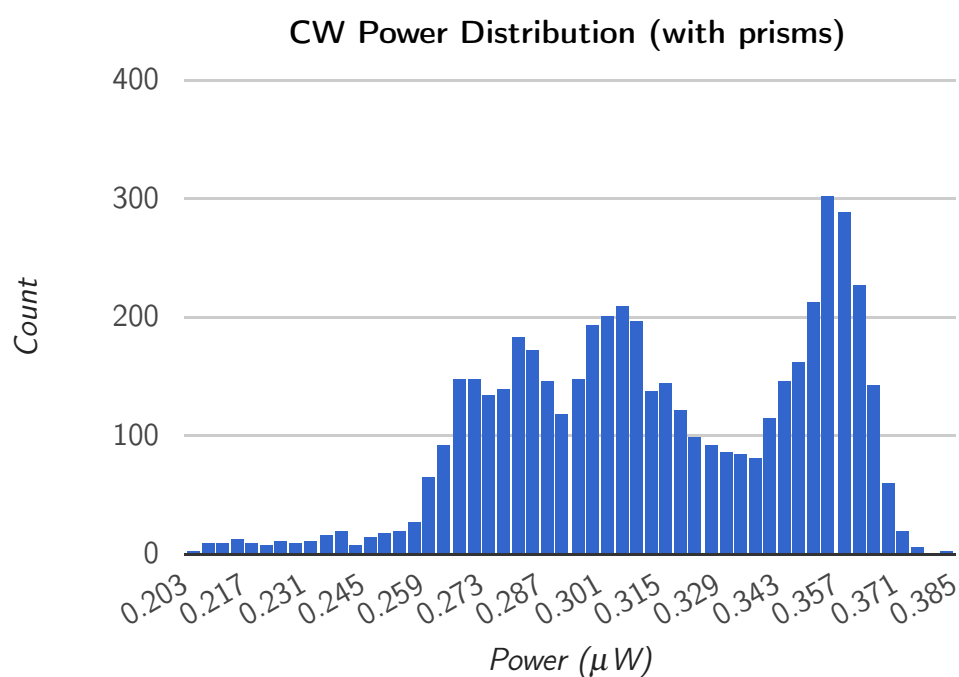


**Figure 3.2 Laser power distribution:** A histogram of the measured power data points. There appears to be a broader lower power peak and a sharper higher power peak. The values of these peaks are close to the average power of the first half of the scan and the average power of the second half of the scan, respectively.

but were unsuccessful. It is possible that by adjusting other mirror locations such a configuration could be achieved but this would be an assignment for a future research student.

# Appendix A

## ABCD Matrix Calculation

Peatross and Ware explain ABCD matrix formalism in their *Optics* text [7]. Each element of an optical setup, including distances between elements, can be expressed as a 2x2 matrix and combined optics are expressed as the product of these matrices. Paraxial rays are expressed as vectors of a ray's distance from and angle with the optical axis and the rays' behaviors are calculated by the inner product of the ABCD matrix and the vector, e.g.  $\begin{bmatrix} A & B \\ C & D \end{bmatrix} \begin{bmatrix} d \\ \theta \end{bmatrix}$ .

In our alternative laser configuration we are only concerned with mirrors and the distances between them, the matrices for which are shown in figures A.1 and A.2. Tables A.1 and A.2 list the distances of focal lengths of elements in the laser and relevant matrices are The entire alternative configuration can be represented as a product of various of both of these matrices corresponding to the optical elements. The stability matrix is shown in figure A.3 while the beam size matrix is shown in figure A.4.

The condition for stability is that the absolute value of the average of the A and D elements of a round-trip (see figure A.3) be less than one. In this case,  $A = -D$ , so this is clearly met. However, we measured the radius of the beam on new HR to be 3.0 mm and it seemed to focus on the flat mirror, corresponding to a ray angle of  $6.016^\circ$ . In order to determine how this ray behaves

$$\begin{bmatrix} 1 & d \\ 0 & 1 \end{bmatrix}$$

**Figure A.1 ABCD matrix for distance  $d$**

$$\begin{bmatrix} 1 & 0 \\ -1/f & 0 \end{bmatrix}$$

**Figure A.2 ABCD matrix for mirror with focal length  $f$**

Distances (mm)

Start	End	Distance	
new HR	flat	284.676	d1
flat	HR A	230	d2
HR A	crystal	50	d3
crystal	HR B	55	d4
HR B	OC	588	d5
HR A	HR B	109.75	d6

**Table A.1 Distances between optical elements:** This table contains the distances in mm between optical elements. Distances are reflexive, i.e.  $X$  to  $Y = Y$  to  $X$ . The distance  $d6$  is the sum of  $d3$  and  $d4$  as well as the length of the crystal. For each element a unique identifier is added to represent the distance matrix in the calculations in figures A.3 and A.4.

Focal lengths (mm)

Mirror	Focal length	
OC	$\infty$	m1
HR A	50	m2
HR B	50	m3
flat	$\infty$	m4
new HR	200	m5

**Table A.2 Focal lengths:** This table contains the focal lengths in mm of the various mirrors. For each mirror a unique identifier is added to represent the focal length matrix in the calculations in figures A.3 and A.4. Note that the flat mirror and OC correspond to an identity matrix.

$$\begin{aligned}
 ABCD &= [d4][m3][d5][m1][d5][m3][d6][m2][d2][m4][d1][m5][d1][m4][d2][m2][d3] \\
 &= \begin{bmatrix} 1.14995 & -6.1527 \text{ mm} \\ 0.377457 \text{ mm}^{-1} & -1.14995 \end{bmatrix}
 \end{aligned}$$

**Figure A.3 Stability ABCD matrix:** This represents a full beam round-trip. By using values in tables A.1 and A.2 and inserting into the matrices in figures A.1 and A.2, the final matrix is obtained with matrix multiplication.

$$\begin{aligned}
 ABCD &= [d5][m3][d6][m2][d2][m4][d1][m5] \\
 &= \begin{bmatrix} 1.23666 & -27.6928 \text{ mm} \\ -0.0001612 \text{ mm}^{-1} & 0.812236 \end{bmatrix}
 \end{aligned}$$

**Figure A.4 Beam size ABCD matrix:** This represents the beam path from new HR to OC. By using values in tables A.1 and A.2 and inserting into the matrices in figures A.1 and A.2, the final matrix is obtained with matrix multiplication.

$$\begin{aligned}
 ABCD * ray &= \begin{bmatrix} 1.23666 & -27.6928 \text{ mm} \\ -0.001612 \text{ mm}^{-1} & 0.812236 \end{bmatrix} \begin{bmatrix} 3.0 \text{ mm} \\ 6.016 \end{bmatrix} \\
 &= \begin{bmatrix} -162.89 \text{ mm} \\ 4.88158 \end{bmatrix}
 \end{aligned}$$

**Figure A.5 Beam size calculation:** By multiplying the paraxial ray vector by the beam size matrix in figure A.4 on the left, we can predict the ray behavior at the output coupler.

at OC, we put these values into a 2-vector and multiplied the beam size matrix on the left (see figure A.5). Unfortunately we see that at the output coupler the beam would have a radius of over 16 cm. When the rays are this far from the optical axis the beam is very faint, difficult to detect, and near impossible to align and achieve lasing.

# Bibliography

- [1] K. Wall and A. Sanchez, “Titanium Sapphire Lasers,” *The Lincoln Laboratory Journal* 9 (1990).
- [2] R. Paschotta, “Mode Locking,” *RP Photonics Encyclopedia* .
- [3] R. Paschotta, “Mode-locked Lasers,” *RP Photonics Encyclopedia* .
- [4] M. M. Murnane and H. C. Kapteyn, *Mode-Locked Ti:Sapphire Laser*, Washington State University, 1994.
- [5] D. C. Smith, “Optical Measurement of Electron Spin Lifetimes in Gallium Arsenide,” Senior thesis (Brigham Young University, Provo, UT, 2011).
- [6] S. Thalman, “Photoluminescence Lifetimes of Quantum Dots,” Senior thesis (Brigham Young University, Provo, UT, 2011).
- [7] J. Peatross and M. Ware, *Physics of Light and Optics*, 2015 ed. (available at [optics.byu.edu](http://optics.byu.edu), 2015).